Title

Preferential remineralization of dissolved organic phosphorus and non-Redfield DOM dynamics in the global ocean: Impacts on marine productivity, nitrogen fixation, and carbon export

Journal

Global Biogeochemical Cycles, 29(3)

ISSN

0886-6236

Authors

Letscher, Robert T

Moore, J Keith

Publication Date

2015-03-01

DOI

10.1002/2014gb004904

AGU PUBLICATIONS

Global Biogeochemical Cycles

RESEARCH ARTICLE
10.1002/2014GB004904

Key Points:
- Marine DOM and its remineralization exhibit non-Redfield C:N:P stoichiometry
- Preferential remineralization of DOP increases marine N2-fixation by 26%
- Marine DOC export increases global export production by 24%

Supporting Information:
- Tables S1 and S2 and Figure S1

Correspondence to:
R. T. Letscher,
robert.letscher@uci.edu

Citation:
Letscher, R. T., and J. K. Moore (2015), Preferential remineralization of dissolved organic phosphorus and non-Redfield DOM dynamics in the global ocean: Impacts on marine productivity, nitrogen fixation, and carbon export, *Global Biogeochem. Cycles*, *29*, 325–340, doi:10.1002/2014GB004904.

Received 27 MAY 2014
Accepted 9 FEB 2015
Accepted article online 13 FEB 2015
Published online 24 MAR 2015

Preferential remineralization of dissolved organic phosphorus and non-Redfield DOM dynamics in the global ocean: Impacts on marine productivity, nitrogen fixation, and carbon export

Robert T. Letscher[1] and J. Keith Moore[1]

[1]Earth System Science, University of California, Irvine, California, USA

Abstract Selective removal of nitrogen (N) and phosphorus (P) from the marine dissolved organic matter (DOM) pool has been reported in several regional studies. Because DOM is an important advective/mixing pathway of carbon (C) export from the ocean surface layer and its non-Redfieldian stoichiometry would affect estimates of marine export production per unit N and P, we investigated the stoichiometry of marine DOM and its remineralization globally using a compiled DOM data set. Marine DOM is enriched in C and N compared to Redfield stoichiometry, averaging 317:39:1 and 810:48:1 for C:N:P within the degradable and total bulk pools, respectively. Dissolved organic phosphorus (DOP) is found to be preferentially remineralized about twice as rapidly with respect to the enriched C:N stoichiometry of marine DOM. Biogeochemical simulations with the Biogeochemical Elemental Cycling model using Redfield and variable DOM stoichiometry corroborate the need for non-Redfield dynamics to match the observed DOM stoichiometry. From our model simulations, preferential DOP remineralization is found to increase the strength of the biological pump by ~9% versus the case of Redfield DOM cycling. Global net primary productivity increases ~10% including an increase in marine nitrogen fixation of ~26% when preferential DOP remineralization and direct utilization of DOP by phytoplankton are included. The largest increases in marine nitrogen fixation, net primary productivity, and carbon export are observed within the western subtropical gyres, suggesting the lateral transfer of P in the form of DOP from the productive eastern and poleward gyre margins may be important for sustaining these processes downstream in the subtropical gyres.

1. Introduction

Marine geochemists have long used the Redfield ratio to link nutrient cycles of nitrogen (N) and phosphorus (P) to fixed carbon (C), allowing quantification of carbon export by applying a fixed ratio of C:N:P for organic matter over regional to global scales. Thus, the Redfield ratio underlies assumptions regarding current estimates of the strength and resiliency of the ocean's biological pump to future perturbations. Dissolved organic matter (DOM) is an important pool within the biological pump, providing an advective/mixing pathway for removal of ~20–25% of global export production [*Hansell et al.*, 2009; *Letscher et al.*, 2015]. Biological production and decomposition of particulate organic matter (POM; size $>0.7\ \mu m$) in the ocean is thought to largely follow the canonical Redfield ratio of 106:16:1 for C:N:P; however, regional deviations from this stoichiometry have recently been documented for both POM [i.e., *Martiny et al.*, 2013a, 2013b] as well as the smaller-sized ($<0.7\ \mu m$) DOM pool [*Clark et al.*, 1998; *Abell et al.*, 2000; *Loh and Bauer*, 2000; *Aminot and Kérouel*, 2004; *Hopkinson and Vallino*, 2005]. These studies have observed DOM to be depleted in P (and N) relative to Redfield proportions in the regions studied (North Pacific, Mediterranean Sea, and North Atlantic), suggesting possible preferential removal of dissolved organic phosphorus (DOP) and nitrogen (DON) during microbial remineralization. Marine DOM depleted in N and P also implies more efficient export of C within DOM compared to POM [*Hopkinson and Vallino*, 2005].

However, the bulk pools of DOM contain both a fraction that is refractory and uniformly mixed throughout the water column and a nonrefractory (degradable) fraction which is labile on some timescale relevant to the timescale of ocean ventilation and overturning circulation [*Carlson*, 2002]. Because these two fractions have very different stoichiometry and lifetimes, *Aminot and Kérouel* [2004] note that the apparent selective removal of N and P with depth could simply be explained by the decreasing proportion of the nonrefractory

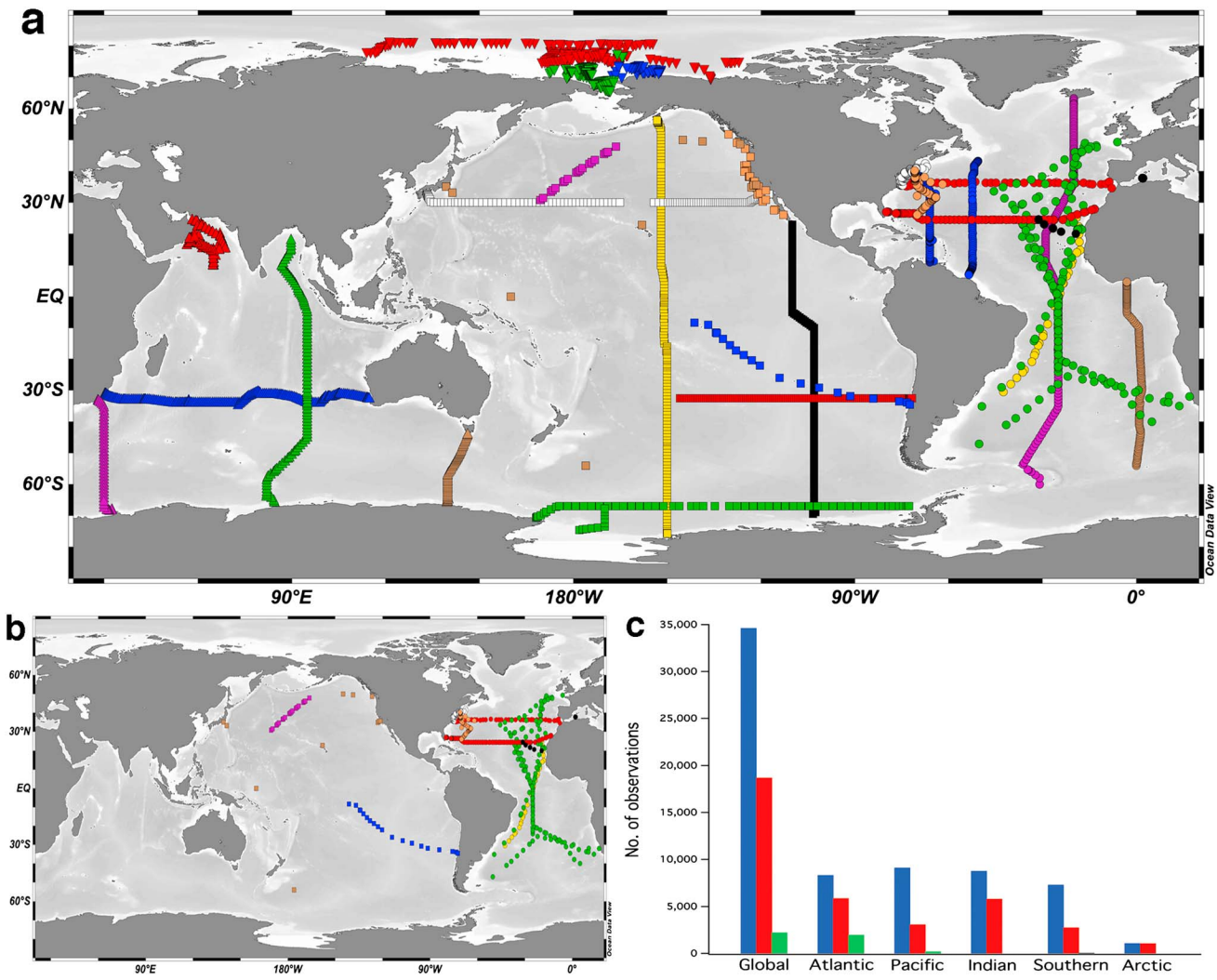

Figure 1. (a) Map depicting sample locations for DOC and DON observations. Most often data covering the full water column depth were available. Definition of colored station locations and corresponding citations are given in supporting information Table S1. (b) The subset of sample locations in Figure 1a that also contains DOP observations. (c) Histogram depicting the distribution of the number of observations of DOC (blue), DON (red), and DOP (green) by ocean basin within the data set.

fraction as it is degraded with depth. In order to examine the stoichiometry of DOM and assess if preferential P remineralization is a global phenomenon, we compiled open ocean observations of marine DOM and calculated molar C:N:P stoichiometries of the DOM pool and its remineralization. This is followed by biogeochemical modeling simulations with the Biogeochemical Elemental Cycling model of the ocean component of the Community Earth System Model that corroborate the need for non-Redfield stoichiometry of DOM cycling to match the observed stoichiometry, thus confirming the preferential remineralization of DOP within the ocean's thermocline at the global scale. Lastly, we discuss the implications of these findings on the magnitude and spatial distribution of marine primary productivity, nitrogen fixation, and the biological pump.

2. Methods

2.1. Data Set and Calculations

We compiled literature and publicly available data of observations of the marine dissolved organic matter pools (dissolved organic carbon (DOC), DON, and DOP). Station locations for observations of DOM included in the data set are shown in Figure 1a, with a smaller subset of these stations containing observations of DOP (Figure 1b). Data coverage spans all five oceans (Atlantic, Pacific, Indian, Arctic, and Southern) (Figure 1c) with

the largest spatial coverage in the Atlantic Ocean (Figure 1a). Observations of DOC and DON are well distributed across the ocean basins; however, DOP observations are concentrated in the Atlantic Ocean (Figures 1b and 1c) and are completely lacking in the Indian, Arctic, and Southern Oceans owing to its omission from many open ocean biogeochemical studies. Notable data gaps for all DOM pools include the Mediterranean Sea and the western Pacific Ocean. Included in the data set are observations of DOM at two ocean time series stations—the Hawaii Ocean Time-series (HOT) in the North Pacific and the Bermuda Atlantic Time-series Station (BATS) in the North Atlantic. Eight continuous years of DOM data were selected from each time series (1993–2000 at HOT; 2001–2008 at BATS) and averaged into eight annual profiles of DOC, DON, and DOP at both stations.

The DOM data are discussed in terms of the characteristics of the bulk pools of DOC, DON, and DOP as well as the nonrefractory (nrDOM) pools. The nrDOM is calculated as the total observed DOM concentration less the concentration of refractory DOM (rDOM) for each pool. As such, our definition of nrDOM contains both the semilabile (lifetime = months to years) and semirefractory (lifetime = decades) fractions of DOM [*Hansell*, 2013]. Histograms for observations of DOM concentrations below 1000 m were found to be normally distributed (supporting information Figure S1); as such the rDOM concentrations were determined by the asymptotic mean concentration of each DOM pool found in the bathypelagic (>1000 m). Deep ocean DOC concentrations were found to vary by basin [e.g., *Hansell and Carlson*, 1998] in the range 38.5–47 μM, while no differences in deep ocean DON (1.8 ± 0.4 μM) and DOP (0.03 ± 0.02 μM) concentrations were discerned, likely due to the larger analytical error of deep ocean DON and DOP determinations [*Hansell*, 1993; *Karl and Björkman*, 2002]. The mean and ±1 standard deviation (SD) of the rDOC concentrations for each basin calculated using normal distribution statistics are reported in supporting information Table S2.

Marine DOM is advected throughout the ocean interior largely along isopycnal surfaces such that depth can be a poor proxy of the extent of aging and accumulated remineralization processes when comparing across ocean basins. Thus, we found it appropriate to bin the DOM data set by neutral density (γ^n) for further analysis of trends in DOM stoichiometry with greater density and along the flow path of interior water masses. Calculation of neutral density requires knowledge of the temperature, salinity, pressure, and geographic location of the water sample [*Jackett and McDougall*, 1997]; however, our compiled DOM data set lacks temperature and salinity data for many of the data. To overcome this limitation, we assigned the climatological monthly average temperature and salinity for each DOM data from the World Ocean Atlas [*Locarnini et al.*, 2013; *Zweng et al.*, 2013] and calculated its neutral density. Neutral density bins had a size of 0.5 kg m^{-3} density units above $\gamma^n = 26.0$, decreasing to 0.2 kg m^{-3} units between $\gamma^n = 26.0$ and 27.6. Below $\gamma^n = 27.5$ (~1000 m), data coverage for DON and DOP was sparse; therefore, only the trends in DOM stoichiometry on neutral density surfaces lighter than $\gamma^n = 27.5$ are included in our analysis.

The stoichiometric ratio of C:N, N:P, and C:P (±1 SD) were calculated using normal distribution statistics following a natural logarithm transformation of the data for both bulk DOM and nrDOM concentrations in each neutral density bin. Additionally, we calculated the Model II reduced major axis regression slope [*Legendre and Legendre*, 1998] between element-element plots of DOC versus DON, DON versus DOP, and DOC versus DOP for nrDOM in each neutral density bin. The slope of the regression between two DOM pools yields information about the net stoichiometry between production and remineralization of each element with respect to the other over the density horizon and environment investigated [*Hopkinson and Vallino*, 2005]. The associated error for each Model II slope is reported as the 95% confidence interval surrounding the calculated slope and is a function of both the residuals variance and the number of data points in each regression.

2.2. Binary Mixing of Thermocline Waters

Following analysis of the global DOM stoichiometry and its remineralization, the data set was subdivided into four ocean basin domains (North/South Atlantic and North/South Pacific) for further investigation of the regional variability in DOM preferential remineralization patterns. At this scale it is necessary to identify the net stoichiometry of DOM remineralization processes that occur within defined water masses, while removing the contribution from mixing of preformed concentrations (inherited from the water mass formation regions) along isopycnal surfaces. We have adopted an approach similar to that found in *Carlson et al.* [2010] in which they applied a binary mixing model of northern and southern component mixing of thermocline waters across the North Atlantic to the investigation of DOC remineralization rates in the mesopelagic realm. For each of the four ocean basins studied we defined neutral density layers for upper thermocline, subtropical mode waters, and lower thermocline water masses and identified end-member or

preformed quantities for potential temperature, salinity, [DOC], [DON], and [DOP] within the source regions for a northern component and a southern component (Table 1). The North Atlantic and North Pacific are bounded by the equator to the south with the southern component source region being defined as ±5°N/S of the equator and the northern component source regions defined as the latitudes where the isopycnals of the respective water masses outcrop at midlatitudes. The South Atlantic and South Pacific are similarly bounded to the north by the equator with the northern component defined at ±5°N/S and the southern component defined at the midlatitude outcrop region. Water mass neutral density ranges for the Atlantic basin are adopted from *Carlson et al*. [2010]; Pacific water mass neutral densities are from *Talley et al*. [2011].

The northern and southern components are most clearly distinguished by differences in potential temperature (θ) for a respective water mass (Table 1), and θ was used in our binary mixing analysis to calculate the fraction of northern versus southern component water in a given thermocline water parcel. The fractions of southern (F_s) and northern (F_n) component water can be calculated as follows:

$$F_s = (\theta^o_n - \theta_{obs})/(\theta^o_n - \theta^o_s) \quad (1)$$

$$F_n = 1 - F_s \quad (2)$$

where θ^o_n and θ^o_s are the end-member θ for the northern and southern components and θ_{obs} is the observed θ for the water parcel. F_n and F_s can be combined with the preformed DOM concentrations for each water mass and component (Table 1) to calculate the preformed concentration (C°) for each observation within the thermocline as follows:

$$C^o = F_n C^o_n + F_s C^o_s \quad (3)$$

where C^o_n and C^o_s are the preformed DOM concentration for the northern and southern components within the water mass of interest. Lastly, the quantity of interest to our analysis, C_{remin}, is the change in DOM concentration due to remineralization processes after removing the contribution from mixing and is calculated as follows:

$$C_{remin} = C_{obs} - C^o \quad (4)$$

where C_{obs} is the observed DOM concentration for the water parcel. For the four ocean basin analysis we calculate the Model II reduced major axis regression slopes using C_{remin} (C_{remin} versus N_{remin}; N_{remin} versus P_{remin}; C_{remin} versus P_{remin}) for each defined thermocline water mass. Also calculated are Model II regression slopes for surface waters (defined as waters with $\gamma^n <$ the top of the upper thermocline layer and/or $<$ 100 m depth) and intermediate water masses (γ^n = 27.0–27.5; Antarctic Intermediate Water in South Pacific north to 15°N, in South Atlantic north to 25°N; North Pacific Intermediate Water in the North Pacific; and Subpolar Mode Water in the North Atlantic).

2.3. Biogeochemical Modeling With the BEC

Model simulations were performed using the Biogeochemical Elemental Cycling (BEC) model, of the ocean component of the Community Earth System Model version 1.2.1 (~3° × ~3° horizontal resolution; 60 vertical levels), which tracks six DOM pools: refractory and semilabile pools for each of DOC, DON, and DOP. DOM cycling in the model has been recently optimized including the fraction of primary productivity that accumulates as DOM, the proportion of this production that is refractory, and the DOM lifetimes based on a data assimilation of, and validation against, the observational DOM data set compiled here [*Letscher et al*., 2015]. DOM is produced within the ecosystem model by phytoplankton growth and grazing at a ratio of ~7% of net primary productivity with a slightly modified Redfield C:N:P ratio of 117:16:1 [*Anderson and Sarmiento*, 1994]. DOM remineralization by bacteria is parameterized by assigned lifetimes for each tracer, which differs between the two model simulations employed in this study. Simulation REDFIELD assigns the optimized DOC parameters to all DOM tracers, routing 1% of DOM production to the refractory DOM pools while assigning the same lifetime (15 years in the euphotic zone, 5.5 years in the mesopelagic) to all semilabile pools; thus, DOM decomposition follows the same 117:16:1 stoichiometry of production. Simulation VAR DOM employs variable stoichiometry for DOM production and remineralization. The fraction of refractory DOM varies as 1% for DOC, 1.15% for DON, and 0.3% for DOP. Semilabile tracers are assigned longer lifetimes (DOC = 15 years; DON = 15 years; DOP = 60 year) in the model's euphotic zone ($<$ ~100 m) and shorter lifetimes (DOC = 5.5 years; DON = 5 years; DOP = 4 years) below. Each phytoplankton group in the BEC model can directly utilize the DOP pool as a P source when phosphate concentrations are low, in line with numerous studies documenting this phenomenon [e.g., *Björkman and Karl*, 2003; *Sohm and Capone*, 2006; *Orchard et al*., 2010]. This process, which

Table 1. Water Mass Definitions and End-Member DOM Concentrations for the Northern Component (NC) and Southern Component (SC) for Each of the Four Ocean Basins[a]

	NC	SC
North Atlantic		
	Upper Thermocline (γ^n (kg m^{-3}) =25.0–26.4)	
Latitude	21.5–26°N	5°S–5°N
θ (°C)	21.83 ± 1.87	18.33 ± 1.87
Salinity	37.04 ± 0.26	35.79 ± 0.12
DOC (μM)	65.3 ± 8.9	55.9 ± 5.7
DON (μM)	4.5 ± 1.0	3.7 ± 0.8
DOP (μM)	0.09 ± 0.06	0.14 ± 0.05
	STMW (γ^n (kg m^{-3}) = 26.4–26.6)	
Latitude	25–32.5°N	5°S–5°N
θ (°C)	17.94 ± 0.46	14.48 ± 0.43
Salinity	36.53 ± 0.10	35.47 ± 0.06
DOC (μM)	53.2 ± 5.0	48.8 ± 2.0
DON (μM)	3.6 ± 0.7	2.8 ± 0.7
DOP (μM)	0.07 ± 0.03	0.16 ± 0.06
	Lower Thermocline (γ^n (kg m^{-3}) = 26.6–27.0)	
Latitude	28–37.5°N	5°S–5°N
θ (°C)	15.30 ± 1.05	12.04 ± 1.15
Salinity	36.09 ± 0.17	35.17 ± 0.14
DOC (μM)	51.0 ± 3.8	46.2 ± 2.0
DON (μM)	3.1 ± 0.9	2.1 ± 0.8
DOP (μM)	0.04 ± 0.03	0.07 ± 0.03
South Atlantic		
	Upper Thermocline (γ^n (kg m^{-3}) = 25.5–26.5)	
Latitude	5°S–5°N	30–41°S
θ (°C)	16.68 ± 1.70	16.50 ± 1.91
Salinity	35.67 ± 0.14	35.46 ± 0.30
DOC (μM)	52.5 ± 3.4	59.0 ± 4.5
DON (μM)	3.3 ± 0.9	4.2 ± 0.6
DOP (μM)	0.15 ± 0.06	0.13 ± 0.04
	STMW (γ^n (kg m^{-3}) = 26.5–26.7)	
Latitude	5°S–5°N	41–48°S
θ (°C)	13.67 ± 0.43	9.95 ± 0.95
Salinity	35.37 ± 0.05	34.44 ± 0.18
DOC (μM)	48.8 ± 2.3	54.4 ± 4.9
DON (μM)	2.7 ± 0.7	3.9 ± 0.6
DOP (μM)	0.10 ± 0.04	0.09 ± 0.03
	Lower Thermocline (γ^n (kg m^{-3}) = 26.7–27.0)	
Latitude	5°S–5°N	49–60°S
θ (°C)	11.49 ± 0.82	6.50 ± 1.02
Salinity	35.10 ± 0.10	34.08 ± 0.11
DOC (μM)	47.0 ± 2.4	48.6 ± 2.6
DON (μM)	2.3 ± 0.8	4.0 ± 0.7
DOP (μM)	0.06 ± 0.03	0.07 ± 0.03

Table 1. (continued)

	NC	SC
	North Pacific	
	Upper Thermocline (γ^n (kg m^{-3}) = 24.0–25.1)	
Latitude	25–35°N	5°S–5°N
θ (°C)	20.20 ± 1.37	21.31 ± 1.33
Salinity	34.91 ± 0.17	35.08 ± 0.28
DOC (μM)	65.3 ± 4.4	55.0 ± 5.0
DON (μM)	4.2 ± 0.4	4.1 ± 0.3
DOP (μM)	0.16 ± 0.06	0.06 ± 0.03
	STMW (γ^n (kg m^{-3}) = 25.1–25.3)	
Latitude	30–45°N	10°S–10°N
θ (°C)	17.68 ± 0.30	19.09 ± 0.73
Salinity	34.79 ± 0.03	35.25 ± 0.22
DOC (μM)	58.1 ± 3.2	54.6 ± 3.7
DON (μM)	4.2 ± 0.5	3.7 ± 1.1
DOP (μM)	0.19 ± 0.05	0.07 ± 0.03
	NPCW (γ^n (kg m^{-3}) = 25.3–26.1)	
Latitude	40–55°N	5°S–5°N
θ (°C)	6.81 ± 1.17	16.32 ± 1.41
Salinity	32.75 ± 0.10	35.03 ± 0.15
DOC (μM)	55.9 ± 1.8	50.9 ± 3.3
DON (μM)	4.3 ± 0.3	3.7 ± 0.8
DOP (μM)	0.17 ± 0.04	0.07 ± 0.03
	Lower Thermocline (γ^n (kg m^{-3}) = 26.1–27.0)	
Latitude	50–55°N	5°S–5°N
θ (°C)	4.16 ± 0.18	11.31 ± 1.48
Salinity	33.41 ± 0.35	34.81 ± 0.10
DOC (μM)	50.8 ± 2.5	46.2 ± 2.4
DON (μM)	4.2 ± 0.3	2.2 ± 0.9
DOP (μM)	0.10 ± 0.03	0.06 ± 0.03
	South Pacific	
	Upper Thermocline (γ^n (kg m^{-3}) = 25.0–25.9)	
Latitude	5°S–5°N	30–40°S
θ (°C)	17.86 ± 0.85	17.29 ± 1.23
Salinity	35.06 ± 0.19	34.98 ± 0.20
DOC (μM)	52.1 ± 3.4	63.1 ± 4.5
DON (μM)	3.8 ± 0.8	4.0 ± 0.6
DOP (μM)	0.07 ± 0.03	0.17 ± 0.03
	STMW (γ^n (kg m^{-3}) = 25.9–26.1)	
Latitude	10°S–10°N	35–45°S
θ (°C)	15.05 ± 0.42	12.34 ± 1.16
Salinity	35.02 ± 0.08	34.24 ± 0.20
DOC (μM)	50.0 ± 1.9	55.7 ± 3.5
DON (μM)	3.3 ± 0.9	3.7 ± 0.7
DOP (μM)	0.07 ± 0.03	0.16 ± 0.03
	Lower Thermocline (γ^n (kg m^{-3}) = 26.1–27.0)	
Latitude	5°S–5°N	45–54°S
θ (°C)	11.31 ± 1.48	8.30 ± 1.17
Salinity	34.81 ± 0.10	34.30 ± 0.14
DOC (μM)	46.2 ± 2.5	49.7 ± 2.1
DON (μM)	2.2 ± 0.9	3.8 ± 0.8
DOP (μM)	0.06 ± 0.03	0.16 ± 0.03

[a]DOM end-member concentrations were calculated as the mean (±1 SD) of data within the reported latitude and neutral density (γ^n) range. STMW = Subtropical Mode Water; NPCW = North Pacific Central Water.

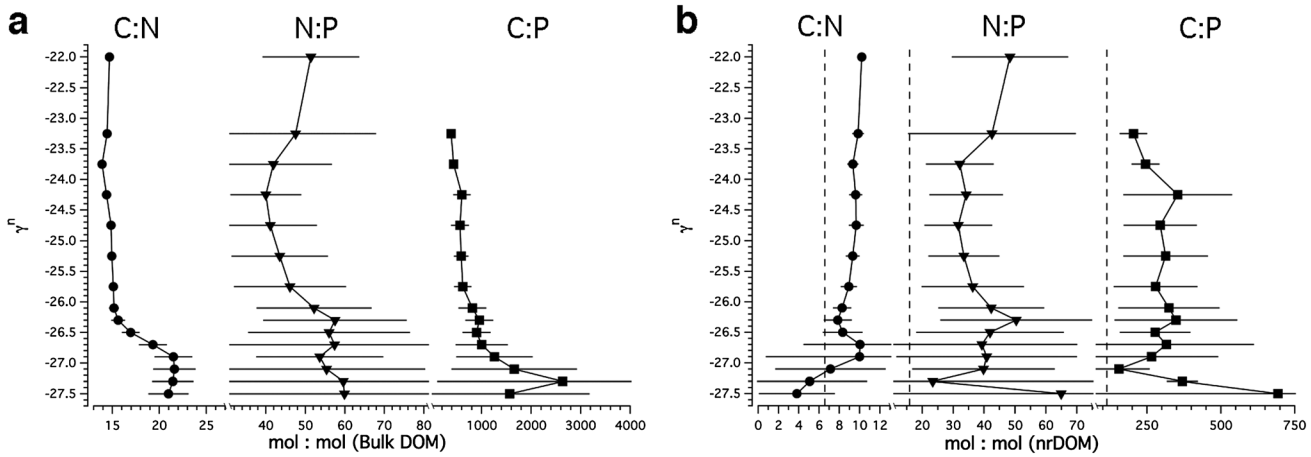

Figure 2. (a) Molar stoichiometry of the bulk DOM pool versus neutral density (γ^n) for DOC:DON, DON:DOP, and DOC:DOP. (b) Molar stoichiometry of the nonrefractory DOM pool versus neutral density (γ^n) for nrDOC:nrDON, nrDON:nrDOP, and nrDOC:nrDOP. Dashed line for each ratio shows the canonical Redfield ratio for reference (C:N = 6.6, N:P = 16, C:P = 106). Error bars for Figures 2a and 2b are ±1 SD.

represents a form of preferential utilization of DOP relative to DOC and DON, is allowed in the VAR DOM simulation but is turned off for the REDFIELD simulation. We perform a third simulation, NO DOPup, which is identical to VAR DOM except that the ability of phytoplankton to directly utilize the DOP pool as a P source is turned off in order to isolate this form of preferential DOP utilization from preferential remineralization by bacteria. A fourth simulation, NO DOM, is also included in which all primary productivity is routed to production of particulate organic matter, eliminating DOM cycling from the ecosystem. Optimization of the DOM parameters and validation of the VAR DOM simulation against observations is detailed elsewhere [*Letscher et al.*, 2015]. BEC simulated semilabile DOM should be considered equivalent to the calculated nrDOM from the observations.

3. Results

3.1. DOM Stoichiometry

In each of the plots that follow, neutral density layers can be related to typical depths/water masses in the water column as follows: Surface waters within the euphotic zone of the low to middle latitudes are found at $\gamma^n = 22.0$–24.0 in the IndoPacific and at $\gamma^n = 22.0$–25.0 in the Atlantic, between the surface waters and the start of the main thermocline at $\gamma^n = 26.0$ lie upper thermocline and mode waters, the main thermocline lies between $\gamma^n = 26.0$ and 27.0, followed by intermediate water masses (e.g., Antarctic Intermediate Water and Subpolar Mode Waters) within $\gamma^n = 27.0$–27.5. The element-element stoichiometric ratios of the bulk DOM pools versus neutral density are shown in Figure 2a. The globally averaged trends fall above the canonical Redfield ratio for all three ratios (C:N, N:P, and C:P) across all density layers. The stoichiometry of each ratio increases within densities of the main thermocline ($\gamma^n = \sim 26.0$–27.0) from values of C:N = ~14.5, N:P = ~45, and C:P = ~530 above to values of C:N = ~21, N:P = ~57, and C:P = ~1600 within the intermediate waters below $\gamma^n = 27.0$.

The element-element ratios for the degradable nrDOM fraction versus neutral density are shown in Figure 2b. The global C:N ratio is greater than Redfield (6.6, dashed line) within the surface and thermocline layers (~9.3 for $\gamma^n < 27.0$) while exhibiting stoichiometry below the Redfield ratio within intermediate waters below. The global N:P and C:P ratios fall above the Redfield ratio across all density layers with nearly constant stoichiometry above $\gamma^n = 27.0$, averaging ~40 for N:P and ~290 for C:P.

3.2. nrDOM Element-Element Regression Slopes

The calculated Model II reduced major axis regression slopes for nrDOM C versus N, N versus P, and C versus P in each neutral density bin are shown in Figure 3. The calculated slopes of C versus N above the main thermocline ($\gamma^n = < 26.0$) are generally higher than the Redfield ratio (dashed line) with values of ~9, indicating that DOC is produced and/or consumed at a ratio greater than Redfield C:N (6.6) in the upper water column. Net C:N remineralization stoichiometry decreases to values below Redfield within the density layers of the main thermocline and below, indicating more rapid N remineralization. N:P production/remineralization

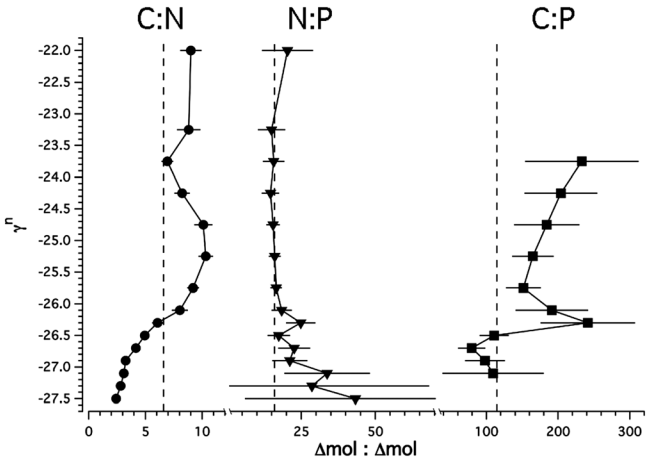

Figure 3. Neutral density (γ^n) profile of the molar stoichiometry of nrDOM remineralization as determined from the slope of the Model II reduced major axis regression for nrDOC versus nrDON, nrDON versus nrDOP, and nrDOC versus nrDOP. Dashed line for each ratio shows the canonical Redfield ratio for reference (C:N = 6.6, N:P = 16, C:P = 106). Error bars are ±95% confidence intervals surrounding the mean estimate of the regression slope and are a function of both data variance and the number of data points within the regression.

stoichiometry closely matches Redfield proportions above the main thermocline with an increase toward more rapid N recycling at deeper densities. Similar to the trend with neutral density observed for C versus N, the slopes of C versus P are elevated with respect to Redfield above the main thermocline (average = ~200 for $\gamma^n = < 26.0$), switching to lower ratios below, indicative of faster P remineralization.

3.3. Preferential Remineralization Patterns of the nrDOM Pool

In order to examine the topic of preferential remineralization (or net production/remineralization processes if within the surface euphotic layer) of one element with respect to another it is necessary to compare the slope of nrDOM element-element regressions with the corresponding in situ nrDOM stoichiometry within each density layer. Figure 4 shows the ratio of the nrDOM element-element stoichiometric ratio to the nrDOM element-element regression slope for the global ocean as well as the four ocean basins. A ratio of unity (dashed line) represents the case of no preferential remineralization of one element with respect to the other; i.e., the stoichiometry of nrDOM remineralization equals the observed in situ nrDOM stoichiometric ratio, while ratios greater than one indicate the relative magnitude of preferential DOP (or DON) remineralization. Phosphorus is found to be preferentially remineralized with respect to both C (Figure 4c) and N (Figure 4b) across nearly all densities and ocean basins investigated in the upper ~1000 m, with an average magnitude of 2.0X versus C and 2.1X versus N. We tested the sensitivity of these estimates given the larger analytical uncertainty in the rDOP concentration, finding that this uncertainty had only a minor effect on the calculated average relative magnitude of preferential DOP remineralization; a ±33% change in the rDOP concentration (i.e., 0.03 ± 0.01 μM) changed the relative magnitude of preferential P versus C remineralization by ± ~9% and preferential P versus N remineralization by ± ~7%. Slight regional differences are observed in the relative magnitude of preferential DOP remineralization with the North Atlantic and South Pacific exhibiting larger relative magnitudes for P versus N remineralization (up to 3.0X; Figure 4b) while the South Atlantic and North Pacific exhibit relative magnitudes near 1.5X. The North Atlantic exhibits the largest relative magnitude of preferential P versus C

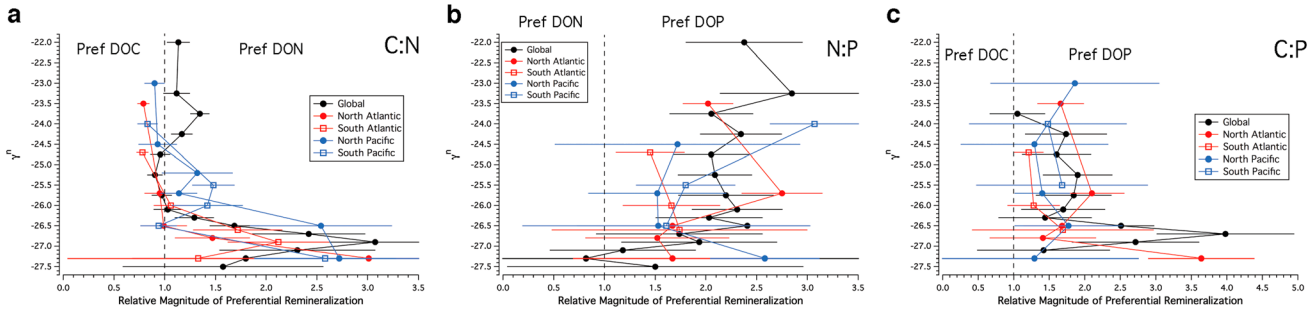

Figure 4. The ratio of the nrDOM pool stoichiometry (from Figure 2b) to the nrDOM remineralization stoichiometry (from Figure 3) plotted versus neutral density (γ^n). The value along the *x* axis provides an estimate of the relative magnitude of preferential remineralization of (a) N versus C, (b) P versus N, and (c) P versus C. A ratio of unity (black dashed line) represents the case for no preferential remineralization, in which the stoichiometry of nrDOM remineralization equals the stoichiometry of the in situ nrDOM pool within a given density layer. Error bars are the propagated error of the nrDOM pool and remineralization stoichiometry calculations. Black circles = Global data set; red filled squares = North Atlantic; red open squares = South Atlantic; blue filled circles = North Pacific; blue open squares = South Pacific.

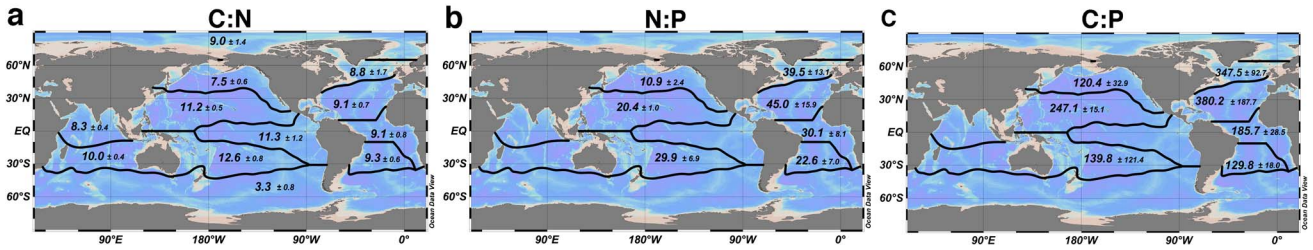

Figure 5. Maps of the nrDOM pool molar stoichiometry binned into twelve biogeochemical provinces, (a) C:N, (b) N:P, and (c) C:P. Borders of the biogeochemical provinces were diagnosed from the surface outcrop of the 0.3 μM [PO_4^{3-}] isoline from the annually averaged World Ocean Atlas [*Garcia et al.*, 2014] to separate the polar regions, subpolar and subtropical gyres, and the equatorial regions. The mean ±95% confidence interval (CI) surrounding the mean of log-transformed nrDOM stoichiometry is reported for the 0–100 m layer.

remineralization (up to 3.5X; Figure 4c), with the other three ocean basins having values near 1.5X. DOC and DON are remineralized in proportions approximately equal to the C:N stoichiometry above the main thermocline ($\gamma^n < 26.0$; Figure 4a), with evidence for preferential remineralization of DON within the thermocline and intermediate layers ($\gamma^n = 26.0$–27.5: Figure 4a) that is common to all four ocean basins investigated.

Having diagnosed regional differences in nrDOM preferential remineralization patterns between the four ocean basins, we chose to investigate the larger scale variability in upper ocean nrDOM stoichiometry across twelve biogeochemical provinces of the global ocean (Figure 5). Significant differences in nrDOM molar stoichiometry were observed both within provinces of the same ocean basin (cf. subpolar North Pacific with the subtropical North Pacific) as well as comparing across ocean basins (cf. the Pacific with the Atlantic). C:N ratios were highest in the Pacific basin (7.5–12.6; Figure 5a) contrasting lower ratios in the Atlantic (8.8–9.3) and Southern Ocean (3.3). The Indian Ocean (8.3–10.0) and Arctic Ocean (9.0) exhibited similar C:N stoichiometry as the Atlantic basin. By contrast, N:P ratios were typically higher in the Atlantic basin (22.6–45.0; Figure 5b) versus lower ratios in the Pacific (10.9–22.9). There is also a pattern of higher ratios found in the subtropical provinces versus the subpolar region of the Pacific basin. The global maximum in N:P (45.0 ± 15.9) was found in the subtropical North Atlantic, consistent with the well-documented P-depleted ecosystem found in this region [e.g., *Ammerman et al.*, 2003] (see section 4 for further discussion). C:P ratios (Figure 5c) were found to vary by latitude similar to results for the N:P ratio. Subtropical gyre C:P was (~247) compared to (~120) for the subpolar gyre in the North Pacific. Atlantic basin C:P increases from south to north across the basin with some decrease in the ratio moving from the subtropical gyre to the subpolar gyre in the North Atlantic. Again the global maximum in C:P (380 ± 188) was observed in the North Atlantic subtropical gyre.

3.4. DOM Stoichiometry Patterns in the BEC Model

Our analysis of the global DOM data set indicates that DOP (and DON with respect to DOC) are preferentially removed from marine DOM upon its remineralization. In addition, the N- and P-poor stoichiometry (in relation to Redfield) of the DOM pools in the upper ocean ($\gamma^n < 26.0$; Figure 2) suggests that marine DOM is either initially produced with a non-Redfield stoichiometry or microbial remineralization in the euphotic zone rapidly removes N and P from DOM. These phenomena have recently been incorporated and optimized for the cycling of DOM in the BEC model [*Letscher et al.*, 2015] for which we will next compare the neutral density resolved DOM stoichiometry between a simulation with the optimized variable DOM cycling stoichiometry, VAR DOM, with a simulation that uses Redfield stoichiometry of DOM cycling, REDFIELD.

The C:N:P stoichiometry of the bulk DOM pools simulated under the REDFIELD and VAR DOM cases are shown in relation to the global C:N:P stoichiometry from observations in Figure 6. VAR DOM C:N (Figure 6a, squares) closely matches the observed stoichiometry (circles) in the upper water column (~15 for $\gamma^n < 26.0$), while the REDFIELD simulation (triangles) exhibits a lower C:N ratio of ~11. Both simulations exhibit increasing C:N ratios with density as is seen in the observations; however, both simulations underestimate the observed stoichiometry by ~20% for REDFIELD and ~10% for VAR DOM. Both REDFIELD and VAR DOM underestimate the observed N:P stoichiometry by ~10–50% in the upper water column ($\gamma^n < 26.0$; Figure 6b); however, only the VAR DOM simulation captures the trend toward increasing ratios at deeper densities visible in the observations. Thus, the shape of the VAR DOM N:P ratio versus neutral density profile is similar to the observations profile albeit shifted to lower values. It is possible that the N:P stoichiometry from the

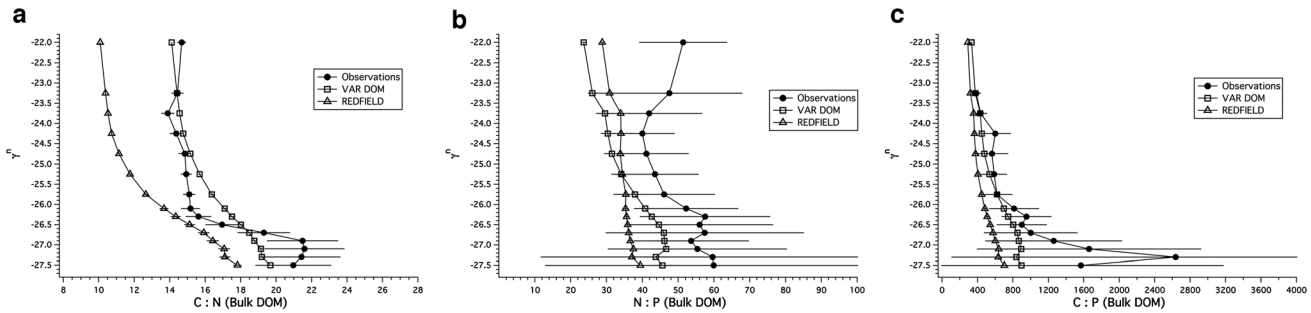

Figure 6. Globally averaged bulk DOM pool stoichiometry versus neutral density (γ^n) for (a) C:N, (b) N:P, and (c) C:P. Results from the REDFIELD (triangles) and VAR DOM (squares) simulations of the BEC model are compared against the observations (circles) from the DOM data set. Error bars are ±95% CI of the mean after log transformation.

observational data set is positively biased owing to the fact that the spatial distribution of DOP observations in the global data set are heavily weighted to the North Atlantic (Figure 1), which was found to have the most P-depleted stoichiometry (Figure 5). The C:P stoichiometry of the VAR DOM simulation (Figure 6c, squares) closely follows that of the observations throughout the upper ocean into the upper thermocline ($\gamma^n < 26.5$; Figure 6c), after which the uncertainty in the C:P stoichiometry of the observations becomes very large. As was the case for the C:N and N:P stoichiometry, the REDFIELD simulation underestimates the observed C:P stoichiometry throughout the investigated densities by ~15–50% (Figure 6c).

3.5. Effects of Variable DOM Stoichiometry on Marine Biogeochemical Processes

We next investigated the effects of non-Redfield DOM dynamics and preferential DOP remineralization on the marine biogeochemical processes of net primary productivity, nitrogen fixation, and carbon export at the global scale by comparison of REDFIELD and VAR DOM in steady state after 310 year simulations. Additional simulations NO DOM and NO DOPup were also performed in order to further isolate the roles that DOM cycling and preferential DOP remineralization in the form of direct utilization by phytoplankton play in the studied biogeochemical processes. Comparison of the globally integrated rates of net primary productivity, nitrogen fixation, and carbon export between the four simulations are found in Table 2.

3.5.1. Net Primary Productivity

Inclusion of variable DOM stoichiometry was found to increase global net primary productivity (NPP) by 10% over the REDFIELD simulation, with ~8% of this increase due to the inclusion of direct DOP uptake by phytoplankton alone and the remaining ~2% due to the variable stoichiometry of DOM production and remineralization. The largest increases in NPP within the VAR DOM simulation, >100%, are found in the low-latitude Atlantic basin (−30°S to 30°N) with additional NPP increases in the western North Pacific subtropics and the subtropical Indian Ocean (Figure 7c). Rates of direct DOP uptake by phytoplankton are highest in these regions in the VAR DOM simulation (not shown), highlighting the role this process plays in providing a source of P to sustain NPP in the oligotrophic subtropical ocean. The simulation with NO DOM exhibited the highest rate of NPP, increasing 20% over the REDFIELD and 10% over the VAR DOM simulations. Productivity increases in the western subtropical Pacific and Indian basins are large enough to outweigh the large decrease in subtropical North Atlantic NPP, which approaches a ~100% decline, as well as additional decreases in Arctic Ocean NPP (Figure 7d). This result highlights the important role that DOM dynamics play in sustaining the majority of simulated productivity in the North Atlantic subtropical gyre as well as a portion of Arctic basin NPP.

Table 2. Globally Integrated Rates of Net Primary Productivity (NPP), Marine Nitrogen Fixation, and Organic Carbon Export From the Four Simulations of the BEC Model[a]

Simulation	NPP	N_2 Fixation	POC_{exp}	DOC_{exp}	Total C_{exp}
REDFIELD	50.9	100.8	6.1	1.9	8.0
VAR DOM	56.0	127.0	6.6	2.1	8.7
NO DOPup	51.8	95.4	6.2	2.0	8.2
NO DOM	61.0	109.5	7.0	0.0	7.0

[a]All units are Pg C yr^{-1} except for N_2 fixation = Tg N yr^{-1}.

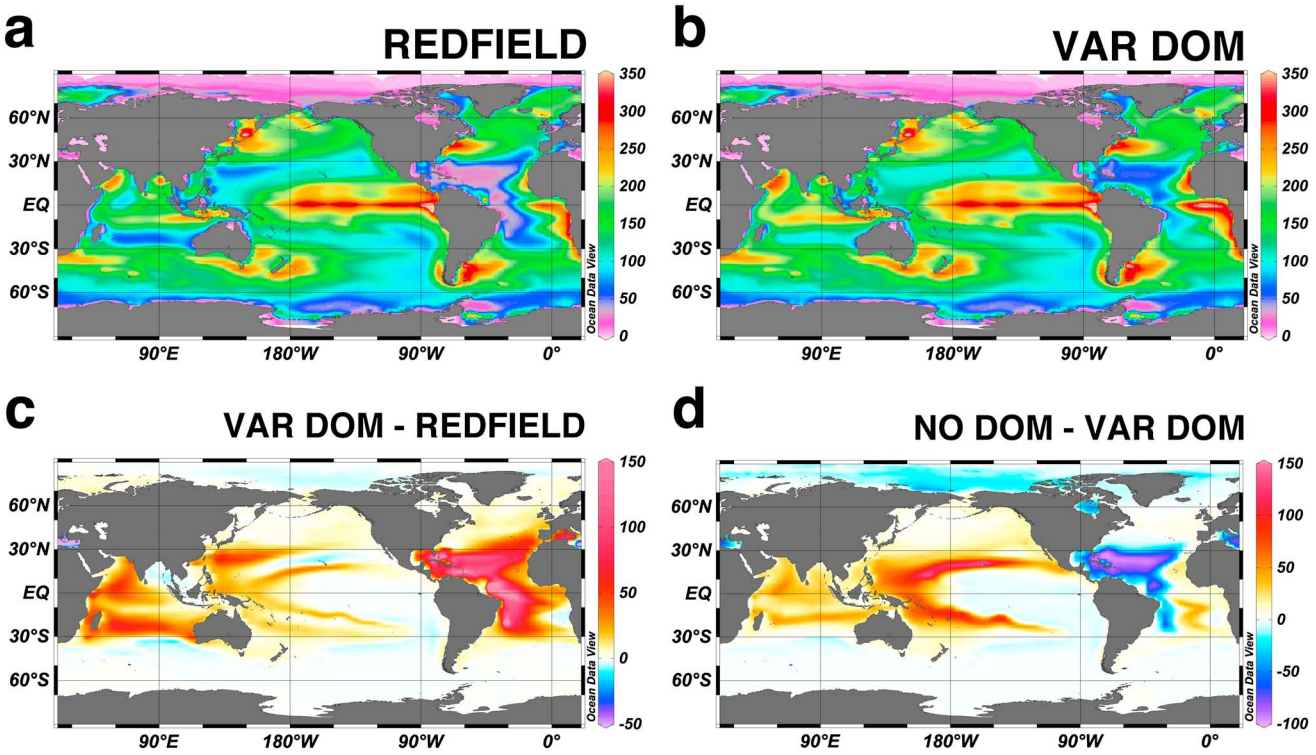

Figure 7. Net primary productivity (NPP; g C m^{-2} yr^{-1}) integrated for the euphotic zone from the (a) REDFIELD and (b) VAR DOM simulations. (c) The difference in NPP rates between the VAR DOM and REDFIELD simulations calculated as a percent. Positive differences (red colors) indicate an increase in NPP for the VAR DOM simulation over REDFIELD. (d) NPP differences between the NO DOM and VAR DOM simulations. Negative differences (blue colors) indicate NPP decreases in the NO DOM simulation over VAR DOM.

3.5.2. Marine N_2 Fixation

Variable DOM cycling stoichiometry was found to impart its largest effect on global rates of marine nitrogen fixation. The VAR DOM simulation had a N_2 fixation rate ~26% greater than REDFIELD, with the largest increases observed in the tropical and subtropical Atlantic, the subtropical Indian, as well as the western subtropical North Pacific basins (Figure 8d). The majority of the observed increase in N_2 fixation can be attributed to the inclusion of direct DOP uptake by phytoplankton in the VAR DOM simulation which increases N_2 fixation by ~33% over the case with variable DOM stoichiometry but no direct DOP uptake (NO DOPup simulation; Table 2). This pathway for P utilization sustains a significant portion of that needed for N_2 fixation in the tropical Atlantic where N_2 fixation rates more than double between the REDFIELD and VAR DOM simulations (Figures 8a, 8b, and 8d). The simulation with NO DOM cycling sustains a similar magnitude of N_2 fixation as REDFIELD (4% higher in NO DOM), although the spatial distribution is greatly altered in the NO DOM case (Figure 8e). Large increases in N_2 fixation in the Indian, western Pacific, and tropical Atlantic basins are partially compensated for by decreases in N_2 fixation in the eastern and central subtropical Pacific and the subtropical North Atlantic.

3.5.3. Carbon Export Below 100 m

We quantified the export of organic carbon below 100 m as a measure of the strength of the ocean's biological carbon pump. Global carbon export is defined as the sum of sinking particulate organic carbon (POC) at 100 m and DOC export below 100 m. The VAR DOM simulation had a globally integrated C export of 8.7 Pg C yr^{-1}, which is ~9% larger than the case with REDFIELD DOM cycling. Two thirds of this increase can be attributed to the inclusion of direct DOP uptake by phytoplankton, with the remaining third due to variable DOM cycling stoichiometry (Table 2). Our export production estimate of 8.7 Pg C yr^{-1} here using the coarser ~3° horizontal resolution BEC model or 9.3 Pg C yr^{-1} at the higher-resolution 1° version of the BEC [*Letscher et al.*, 2015], falls within the range of other estimates, 5–13 Pg C yr^{-1}, produced from model, satellite, and observation based studies [*Boyd and Trull*, 2007; *Dunne et al.*, 2007; *Henson et al.*, 2011; *Westberry et al.*, 2012].

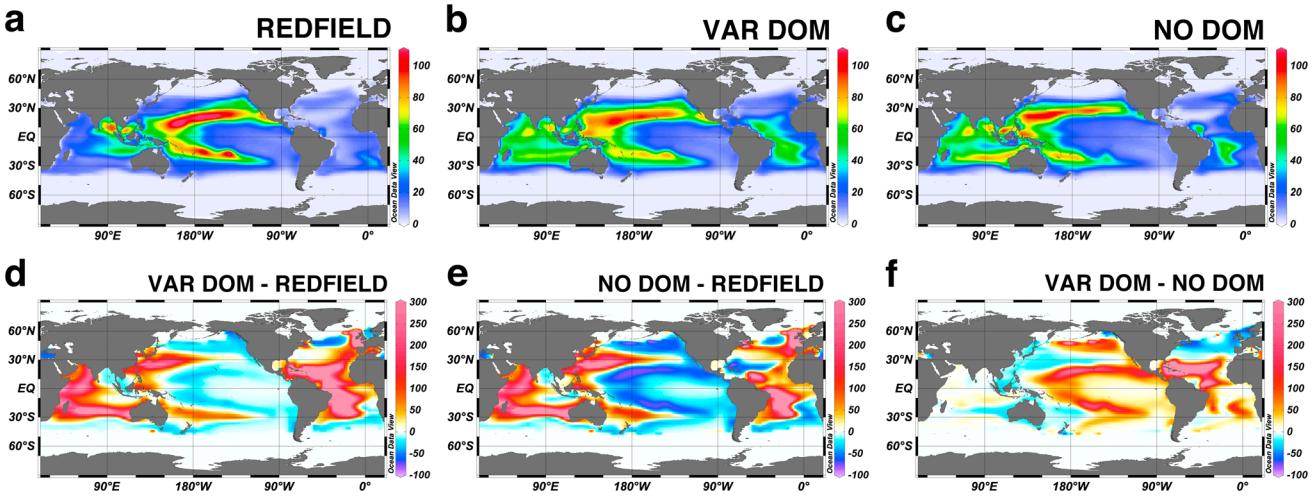

Figure 8. Marine N_2 fixation (mmol N m^{-2} yr^{-1}) integrated for the euphotic zone from the (a) REDFIELD, (b) VAR DOM, and (c) NO DOM simulations. The difference in N_2 fixation rates for (d) VAR DOM minus REDFIELD, (e) NO DOM minus REDFIELD, and (f) VAR DOM minus NO DOM simulations calculated as a percent. In Figures 8d–8f, positive differences (red colors) indicate increases in N_2 fixation in the first listed simulation relative to the second listed.

The spatial pattern of organic carbon export for the BEC simulations is shown in Figure 9. The spatial distribution of C export is broadly similar between the REDFIELD (Figure 9a) and VAR DOM (Figure 9b) simulations; however, the overall global magnitude is larger in VAR DOM (Table 2) with the largest increases found in the western Pacific, Indian Ocean, and especially the tropical and subtropical Atlantic basin (Figure 9c). Carbon export decreases in the subtropical gyre regions of the NO DOM simulation (Figure 9d), especially for the subtropical North Atlantic where C export is <0.5 mol C m^{-2} yr^{-1}, consistent with the large decreases in NPP (Figure 7d) and N_2 fixation (Figure 8c) we observe when DOM cycling is removed from the ecosystem. In order to better illustrate the contribution that DOC export makes to total carbon export and its spatial distribution, we compare C export as consisting of POC export only (Figure 9e) with the contribution of DOC to C export (Figure 9f) from the VAR DOM simulation. DOC export makes its largest contribution to total C export in the

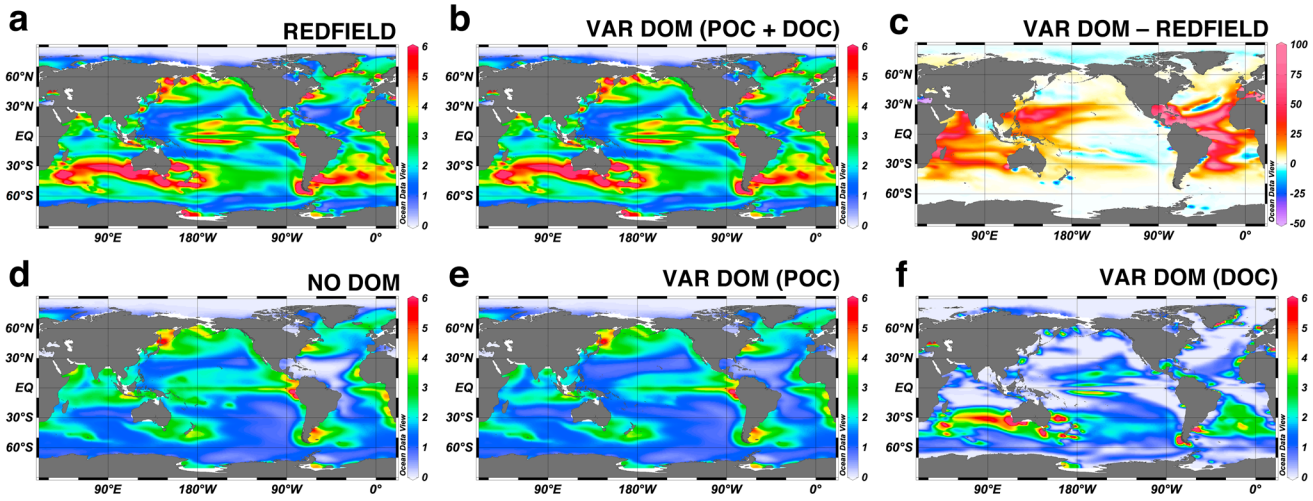

Figure 9. Organic carbon export below 100 m for the (a) REDFIELD and (b) VAR DOM simulations. Carbon export is the sum of POC_{exp} + DOC_{exp} (values reported in Table 2), where POC_{exp} is the sinking flux of POC at 100 m and DOC_{exp} is calculated as the 0–100 m depth normalized [DOC] multiplied by the downward vertical velocity (sum of downward advective and diapycnal mixing terms). (c) The percentage difference in carbon export for the VAR DOM and REDFIELD simulations. Positive differences (red colors) indicate increases in carbon export for the VAR DOM simulation over REDFIELD. Organic carbon export below 100 m for the (d) NO DOM and (e) VAR DOM (POC_{exp} only) simulations. For Figures 9d and 9e carbon export is calculated as POC_{exp} only while omitting DOC_{exp}. (f) Carbon export from DOC_{exp} only for the VAR DOM simulation highlighting the important contribution of DOC_{exp} to total carbon export in the subtropical ocean gyres. All units are mol C m^{-2} yr^{-1} except for Figure 9c (%).

world ocean's subtropical gyres, adding an additional ~0.5–2 mol C m^{-2} yr^{-1}, increasing to ~3–5 mol C m^{-2} yr^{-1} near the equator of the central Pacific, the South Atlantic subtropical gyre, and off the western coast of Australia (Figure 9f).

4. Discussion

4.1. DOM Dynamics With Respect to the Redfield Ratio

In this study we compiled a comprehensive data set of open ocean DOM observations, (>55,000 observations). This DOM data set was used to investigate the C:N:P stoichiometry of both the bulk and degradable marine DOM pools with respect to their similarity or difference to the canonical Redfield stoichiometry of marine nutrient and organic matter pools.

We found bulk DOM stoichiometry consistently above Redfield stoichiometry across all three C:N:P ratios and densities investigated (Figure 2a). The global average C:N:P of bulk DOM is found to be 640:44:1 in the surface ocean ($\gamma^n < 26.0$), increasing to 1070:56:1 in the mesopelagic ($\gamma^n = 26.0$–27.5). Elevated bulk DOM stoichiometry above the Redfield ratio has been observed previously and the gradual increase in positive deviations from Redfield with depth or density (Figure 2a) has traditionally been interpreted as preferential removal of the denominator (N or P) in each ratio with increasing depth/density (and time because waters are older with increasing depth) [*Abell et al.*, 2000; *Aminot and Kérouel*, 2004; *Hopkinson and Vallino*, 2005]. However, by removing the contribution of rDOM to the bulk pool with its elevated stoichiometry, ~1370:60:1, the nrDOM fraction exhibits stoichiometry that varies with respect to its similarity or divergence from the Redfield ratio (Figure 2b). The nrDOM fraction is generally P poor with respect to N and C and N poor with respect to C compared to Redfield proportions. We calculate the global average nrDOM C:N:P stoichiometry to be 317:39:1. This nrDOM stoichiometry is ~200% C rich and ~145% N rich with respect to P and ~25% C rich with respect to N versus Redfieldian organic matter. Thus, marine DOM is found to exhibit non-Redfield C:N:P stoichiometry that is depleted in P and to a secondary degree in N. This could arise from either direct production of P-poor DOM by the surface ocean biology [*Bertilsson et al.*, 2003; *White et al.*, 2006] and its subsequent release into the water column in processes such as sloppy feeding, cell death, and viral lysis or rapid recycling of P from the surface ocean organic matter pools [*Caron*, 1994] such that resident surface ocean DOM is made P poor as it cycles through the microbial loop.

We further investigated the stoichiometry of DOM remineralization by calculating the slope of element-element regressions binned by neutral density. The slopes indicate that globally, nrDOM remineralization more closely follows the Redfield ratio, albeit with a slightly C-rich stoichiometry in the upper water column ($\gamma^n < 26.0$; Figure 3). However, within the main thermocline this C-rich remineralization stoichiometry reverts to more rapid remineralization of P and N ($\gamma^n > 26.0$; Figure 3). We calculate the global C:N:P stoichiometry of nrDOM remineralization to be 165:21:1, similar to the value of 199:20:1 found previously by *Hopkinson and Vallino* [2005].

4.2. Preferential Remineralization Patterns of Marine DOM

Combining the stoichiometries of the marine DOM pool and its remineralization, we evaluated the case for preferential remineralization of the P and N pools. We found P to be preferentially degraded with respect to both N and C across all densities and ocean basins investigated at an average relative magnitude of ~2X. Regional differences in preferential P remineralization patterns were observed with the North Atlantic exhibiting higher relative magnitudes for preferential P remineralization versus both C and N, ~2–3X. The stronger preferential P remineralization behavior within the North Atlantic (Figure 4) may be due in part to the strong phosphorus deficiency present in this basin that has been well documented [*Cotner et al.*, 1997; *Wu et al.*, 2000; *Ammerman et al.*, 2003; *Mather et al.*, 2008] and may point to differing ecosystem functioning between this P-limited system and other less P-stressed ecosystems such as the North Pacific subtropical gyre [*Wu et al.*, 2000]. Our reported C:P and N:P of nrDOM in the upper 100 m of the North Atlantic subtropical gyre of 380:1 and 45:1 (Figure 5) combined with those reported for the suspended particulate organic matter C:P and N:P of ~200:1 and ~35:1 [*Lomas et al.*, 2010; *Martiny et al.*, 2013a], and the inferred C:P of exported sinking organic matter of 355:1 [*Teng et al.*, 2014] all lend further support to this hypothesis that biological cycles in the Sargasso Sea follow a strongly P depleted, non-Redfield stoichiometry. In contrast to the North Atlantic, the relative magnitude of preferential P remineralization

in the other three studied ocean basins is generally lower with values of ~1.5X (Figures 4b and 4c). This suggests less P stress in these ecosystems that is in accord with other observations of gradients in DOP concentrations and alkaline phosphatase activity (a proxy for P stress and DOP utilization) across the Atlantic [*Mather et al*., 2008] and Pacific basins [*Duhamel et al*., 2011].

Carbon was found to be remineralized with a stoichiometry greater than Redfield C:N above the main thermocline (Figure 3); however, the in situ nrC:N molar stoichiometry in the upper ocean is similarly C-rich (Figure 2b) such that no preferential remineralization of C or N occurs (Figure 4a). The C-rich nrDOM and remineralization stoichiometry found at lighter densities possibly point toward an enhanced role for removal of dissolved combined neutral sugars [*Goldberg et al*., 2011], which have been shown to constitute a significant fraction of the DOM preferentially consumed in the upper water column ($<$300 m) in the North Atlantic and North Pacific. The situation shifts in favor of preferential remineralization of N versus C in the main thermocline and below (Figure 4a). Regional differences among the case for preferential remineralization of N versus C are much smaller than the case for preferential P remineralization although the Pacific basins exhibit the shift toward preferential N remineralization at lighter densities ($\gamma^n >$ ~25.0) than is observed in the Atlantic basins ($\gamma^n >$ ~26.0).

We hypothesized that regional differences in preferential remineralization patterns should manifest as regional differences in upper ocean nrDOM molar stoichiometry. There is a general trend toward higher N:P and C:P ratios for the low latitudes and subtropical gyres compared with the higher latitudes, which may be related to the tendency for marine microbes to become C/N rich and P poor at higher temperatures [*Cotner et al*., 2006]. N:P and C:P ratios were also found to be higher (more P depleted) in the Atlantic basin compared to the Pacific (Figure 5). The apparent increase in N:P and C:P ratios from the Southern Hemisphere into the northern Atlantic basin coincide with the northward flow of surface waters in the return flow of the Atlantic meridional overturning circulation, suggesting surface waters gradually become more P depleted as they traverse the Atlantic Ocean, especially through the P-depleted North Atlantic subtropical gyre. C:N ratios were generally higher (more C rich) in the Pacific than in the Atlantic and Indian basins. There is also a trend of higher C:N, N:P, and C:P ratios in the subtropical gyres of the Pacific basin than in the subpolar and polar regions. The anomalously low C:N ratios observed in the Southern Ocean can be attributed to low concentrations of nrDOC in this region as nrDON concentrations were not significantly different in the Southern Ocean compared to other regions.

4.3. Variable Versus Redfield DOM Cycling Stoichiometry in the BEC Model

We tested our findings of preferential remineralization of DOP and DON within simulations of the BEC biogeochemical/ecosystem ocean general circulation model. Comparing simulations with DOM cycling occurring at Redfield and variable stoichiometries, we found that preferential remineralization of DOP and DON were needed to match the observed DOM stoichiometry above $\gamma^n = 27.5$ (i.e., the upper ~1000 m). The observed C:N:P stoichiometry of DOM is relatively constant at the lighter densities of the upper ocean then rapidly increases in the main thermocline and intermediate water masses ($\gamma^n > 26.0$; Figure 6, circles), which can be partially attributed to the finding that DOP and DON are preferentially remineralized with respect to C (from Figure 4). As N is preferentially remineralized with respect to C, and P is preferentially remineralized with respect to both N and C, the faster turnover of P and N results in increasing ratios of C:N, N:P, and C:P within and below the ocean's thermocline. The VAR DOM simulation which contains faster turnover for DOP and DON than DOC is able to capture the increasing C:N:P stoichiometry with density trend (Figure 6; squares). On the other hand, although DOM cycling following Redfield stoichiometry also exhibited increasing ratios with density, the REDFIELD simulation consistently underestimated the observed DOM stoichiometry across all densities and all three ratios of C:N:P (Figure 6; triangles). This finding confirms the supposition held by *Aminot and Kéroue*l [2004] that the decreasing proportion of nrDOM and increasing proportion of rDOM (with its greatly N and P depleted stoichiometry, ~1370:60:1) to the total DOM pool with depth (density) can lead to increasing C:N:P stoichiometry, which can wrongfully be interpreted as preferential remineralization of DON and DOP. Only the combination of the decreasing proportion of nrDOM with depth (density) and faster turnover of DOP and DON than DOC can match the observed DOM C:N:P stoichiometry; i.e., the VAR DOM simulation (Figure 6).

Next, we investigated the effects that variable DOM cycling stoichiometry and preferential DOP and DON remineralization have on the magnitude and spatial pattern of global scale biogeochemical processes. Net

primary productivity was found to increase by 10% when variable DOM cycling is included, with the largest increases observed in the subtropical Atlantic, western Pacific, and western Indian basins. This spatial pattern suggests the lateral supply of N and P from the more productive eastern and poleward sides of the basins as well as the ability of phytoplankton to directly utilize DOP as a P source in the VAR DOM scenario are important nutrient supply mechanisms supporting elevated rates of NPP downstream in the gyre. This process appears to be of particular importance in the subtropical North Atlantic, where in the NO DOM simulation, NPP nearly ceases in this region when the role of DOM as an advective nutrient supply mechanism to the region is turned off, consistent with field studies suggesting a key role for DOP in this ecosystem [e.g., *Lomas et al*., 2010; *Sohm and Capone*, 2010].

Global marine N_2 fixation is 26% greater when variable DOM cycling stoichiometry is considered over the case of Redfield. The spatial pattern of observed increases mirrors that found for NPP, demonstrating that much of the increases to NPP in these regions are due to increases in N_2 fixation. Therefore, preferential remineralization of DOP acts to increase the niche of diazotrophs by decreasing the N:P ratio of the inorganic nutrient pools as P is remineralized at a more rapid rate than N. Preferential remineralization of P in the form of direct utilization of DOP by phytoplankton further decrease the N:P ratio of surface waters. This process is especially important in the Atlantic basin where even though elevated concentrations of dissolved Fe exist in surface waters, significant rates of N_2 fixation are only observed when variable DOM cycling stoichiometry is considered in our simulations versus the cases of Redfield or no DOM cycling.

Including the contribution of organic carbon export due to DOC export increases the strength of the ocean's biological carbon pump by ~14% if DOM cycling follows Redfield stoichiometry. Including our finding of variable DOM stoichiometry increases the strength of the biological pump further by an additional ~9%; thus, DOC export contributes ~24% of global export production. The largest changes in carbon export when DOC export is considered are found within the subtropical ocean gyres, highlighting the dual importance of these regions acting as large reservoirs for surface accumulated DOC and sites of downwelling circulation for the advective removal of surface ocean-accumulated DOC. We observe the percentage of total carbon export contributed by DOC export to be larger near the HOT time series station in the North Pacific than at the BATS station in the North Atlantic (Figure 9f), in agreement with a recent analysis of the relative contributions of sinking POC and DOC export at these sites [*Emerson*, 2014].

5. Conclusion

Many of our current estimates of the strength of the biological carbon pump rely on models that assume organic matter and its export to follow the Redfield ratio. However, our study demonstrates that marine DOM does not follow this stoichiometry and instead P and N are selectively degraded yielding a C-rich composition of the remaining DOM relative to Redfield. Including these processes in the BEC ocean biogeochemistry model, we find a ~9% larger estimate of global C export (8.7 Pg C yr^{-1}) over the case for DOM cycling at Redfield proportions. Preferential remineralization of DOP also increases the niche for diazotrophs, stimulating elevated rates of nitrogen fixation. Future studies examining the strength and resiliency of the ocean's biological pump and other biogeochemical processes to climate change need to consider the effects of non-Redfield stoichiometry in the organic matter pools, including a reevaluation of particulate organic matter stoichiometry given its larger importance to C export.

Acknowledgments

The authors would like to thank the tireless efforts of the international team of scientists, crew, and funding agencies involved in the collection, analysis, and production of the DOM observations used in our analysis. We are especially grateful for the sharing of DOP data from the British Oceanographic Data Centre and all of the PIs involved including Claire Mahaffey, Sinhue Torres-Valdés, Xi Pan, Malcolm Woodward, Rhiannon Mather, Angela Landolfi, and Richard Sanders. The collated DOM data set can be accessed upon request from the corresponding author (robert.letscher@uci.edu), also requiring a separate license for select Atlantic Ocean DOM data from the BODC (http://www.bodc.ac.uk/). This work was supported by grant ER65358 from the U.S. Department of Energy Office of Biological and Environmental Research to J.K.M. J.K.M. also acknowledges support from the National Science Foundation grants AGS-1021776 and AGS-1048890.

References

Abell, J., S. Emerson, and P. Renaud (2000), Distributions of TOP, TON and TOC in the North Pacific subtropical gyre: Implications for nutrient supply in the surface ocean and remineralization in the upper thermocline, *J. Mar. Res.*, *58*(2), 203–222, doi:10.1357/002224000321511142.

Aminot, A., and R. Kérouel (2004), Dissolved organic carbon, nitrogen and phosphorus in the NE Atlantic and the NW Mediterranean with particular reference to non-refractory fractions and degradation, *Deep Sea Res., Part I*, *51*(12), 1975–1999, doi:10.1016/j.dsr.2004.07.016.

Ammerman, J. W., R. R. Hood, D. A. Case, and J. B. Cotner (2003), Phosphorus deficiency in the Atlantic: An emerging paradigm in oceanography, *Eos Trans. AGU*, *84*(18), 165–170, doi:10.1029/2003EO180001.

Anderson, L. A., and J. L. Sarmiento (1994), Redfield ratios of remineralization determined by nutrient data analysis, *Global Biogeochem. Cycles*, *8*(1), 65–80, doi:10.1029/93GB03318.

Bertilsson, S., O. Berglund, D. M. Karl, and S. W. Chisholm (2003), Elemental composition of marine Prochlorococcus and Synechococcus: Implications for the ecological stoichiometry of the sea, *Limnol. Oceanogr.*, *48*(5), 1721–1731.

Björkman, K. M., and D. M. Karl (2003), Bioavailability of dissolved organic phosphorus in the euphotic zone at Station ALOHA, North Pacific Subtropical Gyre, *Limnol. Oceanogr.*, *48*(3), 1049–1057.

Boyd, P. W., and T. W. Trull (2007), Understanding the export of biogenic particles in oceanic waters: Is there consensus?, *Prog. Oceanogr.*, *72*(4), 276–312, doi:10.1016/j.pocean.2006.10.007.
Carlson, C. A. (2002), Production and removal processes, in *Biogeochemistry of Marine Dissolved Organic Matter*, 1st ed., edited by D. A. Hansell and C. A. Carlson, pp. 91–151, Academic Press, San Diego, Calif., doi:10.1016/B978-012323841-2/50007-5.
Carlson, C. A., D. A. Hansell, N. B. Nelson, D. A. Siegel, W. M. Smethie, S. Khatiwala, M. M. Meyers, and E. Halewood (2010), Dissolved organic carbon export and subsequent remineralization in the mesopelagic and bathypelagic realms of the North Atlantic basin, *Deep Sea Res., Part II*, *57*, 1433–1445.
Caron, D. A. (1994), Inorganic nutrients, bacteria, and the microbial loop, *Microb. Ecol.*, *28*(2), 295–298, doi:10.1007/BF00166820.
Clark, L. L., E. D. Ingall, and R. Benner (1998), Marine phosphorus is selectively remineralized, *Nature*, *393*(6684), 426–426, doi:10.1038/30881.
Cotner, J. B., J. W. Ammerman, E. R. Peele, and E. Bentzen (1997), Phosphorus-limited bacterioplankton growth in the Sargasso Sea, *Aquat. Microb. Ecol.*, *13*(2), 141–149, doi:10.3354/ame013141.
Cotner, J. B., W. Makino, and B. A. Biddanda (2006), Temperature affects stoichiometry and biochemical composition of Escherichia coli, *Microb. Ecol.*, *52*(1), 26–33.
Duhamel, S., K. M. Björkman, F. Van Wambeke, T. Moutin, and D. M. Karl (2011), Characterization of alkaline phosphatase activity in the North and South Pacific Subtropical Gyres: Implications for phosphorus cycling, *Limnol. Oceanogr.*, *56*(4), 1244–1254, doi:10.4319/lo.2011.56.4.1244.
Dunne, J. P., J. L. Sarmiento, and A. Gnanadesikan (2007), A synthesis of global particle export from the surface ocean and cycling through the ocean interior and on the seafloor, *Global Biogeochem. Cycles*, *21*, GB4006, doi:10.1029/2006GB002907.
Emerson, S. (2014), Annual net community production and the biological carbon flux in the ocean, *Global Biogeochem. Cycles*, *28*, 14–28, doi:10.1002/2013GB004680.
Garcia, H. E., R. A. Locarnini, T. P. Boyer, J. I. Antonov, O. K. Baranova, M. M. Zweng, J. Reagan, and D. R. Johnson (2014), *World Ocean Atlas 2013, Volume 4: Dissolved Inorganic Nutrients (Phosphate, Nitrate, Silicate)*, *NOAA Atlas NESDIS*, vol. 76, edited by S. Levitus, 25 pp., U.S. Gov. Print. Off., Washington, D. C.
Goldberg, S. J., C. A. Carlson, M. Brzezinski, N. B. Nelson, and D. A. Siegel (2011), Systematic removal of neutral sugars within dissolved organic matter across ocean basins, *Geophys. Res. Lett.*, *38*, L17606, doi:10.1029/2011GL048620.
Hansell, D. A. (1993), Results and observations from the measurement of DOC and DON in seawater using a high-temperature catalytic oxidation technique, *Mar. Chem.*, *41*(1), 195–202, doi:10.1016/0304-4203(93)90119-9.
Hansell, D. A. (2013), Recalcitrant dissolved organic carbon fractions, *Annu. Rev. Mar. Sci.*, *5*, 421–445, doi:10.1146/annurev-marine-120710-100757.
Hansell, D. A., and C. A. Carlson (1998), Deep-ocean gradients in the concentration of dissolved organic carbon, *Nature*, *395*(6699), 263–266, doi:10.1038/26200.
Hansell, D. A., C. A. Carlson, D. J. Repeta, and R. Schlitzer (2009), Dissolved organic matter in the ocean: A controversy stimulates new insights, *Oceanography*, *22*(4), 202–211, doi:10.5670/oceanog.2009.109.
Henson, S. A., R. Sanders, E. Madsen, P. J. Morris, F. Le Moigne, and G. D. Quartly (2011), A reduced estimate of the strength of the ocean's biological carbon pump, *Geophys. Res. Lett.*, *38*, L04606, doi:10.1029/2011GL046735.
Hopkinson, C. S., and J. J. Vallino (2005), Efficient export of carbon to the deep ocean through dissolved organic matter, *Nature*, *433*(7022), 142–145, doi:10.1038/nature03191.
Jackett, D. R., and T. J. McDougall (1997), A neutral density variable for the world's oceans, *J. Phys. Oceanogr.*, *27*, 237–263.
Karl, D. M., and K. M. Björkman (2002), Dynamics of DOP, in *Biogeochemistry of Marine Dissolved Organic Matter*, 1st ed., edited by D. A. Hansell and C. A. Carlson, pp. 249–366, Academic Press, San Diego, Calif., doi:10.1016/B978-012323841-2/50007-5.
Legendre, P., and L. Legendre (1998), Number 20 in Developments in environmental modelling, in *Numerical Ecology*, 2nd ed., Elsevier, Amsterdam.
Letscher, R. T., J. K. Moore, Y. C. Teng, and F. Primeau (2015), Variable C:N:P stoichiometry of dissolved organic matter cycling in the Community Earth System Model, *Biogeosciences*, *12*, 209–221, doi:10.5194/bg-12-209-2015.
Locarnini, R. A., et al. (2013), *World Ocean Atlas 2013, Volume 1: Temperature*, *NOAA Atlas NESDIS*, vol. 73, edited by S. Levitus, 40 pp., U.S. Gov. Print. Off., Washington, D. C.
Loh, A. N., and J. E. Bauer (2000), Distribution, partitioning and fluxes of dissolved and particulate organic C, N and P in the eastern North Pacific and Southern Oceans, *Deep Sea Res., Part I*, *47*(12), 2287–2316, doi:10.1016/S0967-0637(00)00027-3.
Lomas, M. W., A. L. Burke, D. A. Lomas, D. W. Bell, C. Shen, S. T. Dyhrman, and J. W. Ammerman (2010), Sargasso Sea phosphorus biogeochemistry: An important role for dissolved organic phosphorus (DOP), *Biogeosciences*, *7*(2), 695–710.
Martiny, A. C., C. T. Pham, F. W. Primeau, J. A. Vrugt, J. K. Moore, S. A. Levin, and M. W. Lomas (2013a), Strong latitudinal patterns in the elemental ratios of marine plankton and organic matter, *Nat. Geosci.*, *6*(4), 279–283, doi:10.1038/ngeo1757.
Martiny, A. C., J. A. Vrugt, F. W. Primeau, and M. W. Lomas (2013b), Regional variation in the particulate organic carbon to nitrogen ratio in the surface ocean, *Global Biogeochem. Cycles*, *27*, 723–731, doi:10.1002/gbc.20061.
Mather, R. L., S. E. Reynolds, G. A. Wolff, R. G. Williams, S. Torres-Valdes, E. M. S. Woodward, A. Landolfi, X. Pan, R. Sanders, and E. P. Achterberg (2008), Phosphorus cycling in the North and South Atlantic Ocean subtropical gyres, *Nat. Geosci.*, *1*(7), 439–443, doi:10.1038/ngeo232.
Orchard, E. D., J. W. Ammerman, M. W. Lomas, and S. T. Dyhrman (2010), Dissolved inorganic and organic phosphorus uptake in Trichodesmium and the microbial community: The importance of phosphorus ester in the Sargasso Sea, *Limnol. Oceanogr.*, *55*(3), 1390–1399.
Sohm, J. A., and D. G. Capone (2006), Phosphorus dynamics of the tropical and subtropical north Atlantic: Trichodesmium spp. versus bulk plankton, *Mar. Ecol. Prog. Ser.*, *317*, 21.
Sohm, J. A., and D. G. Capone (2010), Zonal differences in phosphorus pools, turnover and deficiency across the tropical North Atlantic Ocean, *Global Biogeochem. Cycles*, *24*, GB2008, doi:10.1029/2008GB003414.
Talley, L. D., G. L. Pickard, W. J. Emery, and J. H. Swift (2011), Pacific Ocean, in *Descriptive Physical Oceanography An Introduction*, 6th ed., edited by L. D. Talley et al., pp. 303–362, Elsevier, San Diego, Calif.
Teng, Y. C., F. W. Primeau, J. K. Moore, M. W. Lomas, and A. C. Martiny (2014), Global-scale variations of the ratios of carbon to phosphorus in exported marine organic matter, *Nat. Geosci.*, doi:10.1038/ngeo2303, in press.
Westberry, T. K., P. J. L. B. Williams, and M. J. Behrenfeld (2012), Global net community production and the putative net heterotrophy of the oligotrophic oceans, *Global Biogeochem. Cycles*, *26*, GB4019, doi:10.1029/2011GB004094.
White, A. E., Y. Spitz, D. Karl, and R. M. Letelier (2006), Flexible elemental stoichiometry in Trichodesmium spp. and its ecological implications, *Limnol. Oceanogr.*, *51*(4), 1777–1790.
Wu, J., W. Sunda, E. A. Boyle, and D. M. Karl (2000), Phosphate depletion in the western North Atlantic Ocean, *Science*, *289*(5480), 759–762, doi:10.1126/science.289.5480.759.
Zweng, M. M., et al. (2013), *World Ocean Atlas 2013, Volume 2: Salinity*, *NOAA Atlas NESDIS*, vol. 74, edited by S. Levitus, 39 pp., U.S. Gov. Print. Off., Washington, D. C.